This article is a *Plant Cell* Advance Online Publication. The date of its first appearance online is the official date of publication. The article has been edited and the authors have corrected proofs, but minor changes could be made before the final version is published. Posting this version online reduces the time to publication by several weeks.

The Phragmoplast-Orienting Kinesin-12 Class Proteins Translate the Positional Information of the Preprophase Band to Establish the Cortical Division Zone in *Arabidopsis thaliana*[C][W]

Elisabeth Lipka,[a] Astrid Gadeyne,[b,c] Dorothee Stöckle,[a] Steffi Zimmermann,[a] Geert De Jaeger,[b,c] David W. Ehrhardt,[d] Viktor Kirik,[e] Daniel Van Damme,[b,c] and Sabine Müller[a,1]

[a] Center for Plant Molecular Biology, ZMBP, Developmental Genetics, University of Tübingen, 72076 Tübingen, Germany
[b] Department of Plant Systems Biology, VIB, B-9052 Gent, Belgium
[c] Department of Plant Biotechnology and Bioinformatics, Ghent University, B-9052 Gent, Belgium
[d] Department of Plant Biology, Carnegie Institution for Science, Stanford, California 94305
[e] School of Biological Sciences, Illinois State University, Normal, Illinois 61790

The preprophase band (PPB) is a faithful but transient predictor of the division plane in somatic cell divisions. Throughout mitosis the PPBs positional information is preserved by factors that continuously mark the division plane at the cell cortex, the cortical division zone, by their distinct spatio-temporal localization patterns. However, the mechanism maintaining these identity factors at the plasma membrane after PPB disassembly remains obscure. The pair of kinesin-12 class proteins PHRAGMOPLAST ORIENTING KINESIN1 (POK1) and POK2 are key players in division plane maintenance. Here, we show that POK1 is continuously present at the cell cortex, providing a spatial reference for the site formerly occupied by the PPB. Fluorescence recovery after photobleaching analysis combined with microtubule destabilization revealed dynamic microtubule-dependent recruitment of POK1 to the PPB during prophase, while POK1 retention at the cortical division zone in the absence of cortical microtubules appeared static. POK function is strictly required to maintain the division plane identity factor TANGLED (TAN) after PPB disassembly, although POK1 and TAN recruitment to the PPB occur independently during prophase. Together, our data suggest that POKs represent fundamental early anchoring components of the cortical division zone, translating and preserving the positional information of the PPB by maintaining downstream identity markers.

INTRODUCTION

The plant microtubule (MT) cytoskeleton demonstrates remarkable plasticity in its ability to form complex arrays characteristic of distinct cell cycle phases and required for specific cellular functions. In expanding interphase cells, parallel aligned cortical MTs guide cellulose synthase complexes along transverse trajectories and permit cell expansion in a perpendicular direction (Paredez et al., 2006). Furthermore, vascular plants developed a specialized cytoskeletal array aiding the correct positional execution of cytokinesis. Entry into mitosis is characterized by the preprophase band (PPB) (Pickett-Heaps and Northcote, 1966), an equatorial assembly of actin filaments and cortical MTs shaped by differential modulation of MT dynamic instability and selective MT stabilization in distinct regions of the cell cortex (Dhonukshe and Gadella, 2003; Vos et al., 2004). PPB formation requires the enzymatic action of a PP2A phosphatase holoenzyme complex containing FASS as a regulatory B subunit, complexed with the helper/assembly proteins TON1a and b, which is targeted to the MTs via the Tonneau Recruitment Motif proteins (Spinner et al., 2013). However, the PPB persists only transiently until pro-metaphase when its disassembly fuels the polymerization of spindle MT. After chromosome segregation and the subsequent condensation of daughter nuclei, the cytokinetic phragmoplast, a dual array of parallel-oriented MTs connecting at the cell division plane, evolves from the anaphase spindle remnants and assists in the synthesis of the cell plate, a de novo established membrane compartment generated by transport and fusion of endomembrane derived vesicles to the division plane, to bisect the daughter cells. The cell plate grows centrifugally and physically separates the daughter nuclei upon fusion with the plasma membrane at the end of plant cytokinesis. Intriguingly, the PPB anticipates the site of fusion between the cell plate and the parental cell wall despite the considerable time lag between the PPB's disassembly at pro-metaphase and the end of cytokinesis when the position of the PPB is converted into the actual cell plate position (Gunning and Wick, 1985).

The correlation between PPB position and the site of cell plate fusion led to the hypothesis that the PPB determines the plane of cell division and recruits molecules that serve as positional information to establish and maintain the cortical division zone

[1] Address correspondence to sabine.mueller@zmbp.uni-tuebingen.de. The author responsible for distribution of materials integral to the findings presented in this article in accordance with the policy described in the Instructions for Authors (www.plantcell.org) is: Sabine Müller (sabine.mueller@zmbp.uni-tuebingen.de).
[C] Some figures in this article are displayed in color online but in black and white in the print edition.
[W] Online version contains Web-only data.
www.plantcell.org/cgi/doi/10.1105/tpc.114.124933

(CDZ) identity throughout mitosis (reviewed in Rasmussen et al., 2013). However, the first proteins described to serve as a reference beyond PPB disassembly were negative markers such as F-actin (Mineyuki and Palevitz, 1990; Cleary et al., 1992) and later the *Arabidopsis thaliana* kinesin-14 KCA1, both characterized by their low protein abundance or deficiency at the CDZ (Sano et al., 2005; Vanstraelen et al., 2006). In *Arabidopsis*, the microtubule binding protein TANGLED (TAN) and the Ran GTPase regulatory protein RanGAP1 both colocalize with the PPB and remain at the CDZ throughout mitosis (Walker et al., 2007; Xu et al., 2008). During the course of mitosis, the CDZ seems to alter from an initially wide zone (the CDZ) to a narrow site (cortical division site [CDS]) at the end of cytokinesis (Van Damme, 2009). The initial recruitment of both TAN and RanGAP1 to the cell cortex requires PPB formation (Walker et al., 2007; Xu et al., 2008), whereas TAN residency at the CDZ/CDS post PPB disassembly does not require MTs (Walker et al., 2007). In *Arabidopsis*, both TAN and RanGAP1 maintenance at the CDZ is abolished in a mutant background lacking a pair of kinesin-12 proteins, PHRAGMOPLAST ORIENTING KINESIN1 (POK1) and POK2 (Walker et al., 2007; Xu et al., 2008). *Arabidopsis pok1 pok2* double mutants display severe cell wall positioning defects, reminiscent of the maize (*Zea mays*) *tan1* phenotype (Smith et al., 1996). The majority of phragmoplasts in the *pok1 pok2* double mutant do not correspond to a transverse orientation relative to the cell longitudinal axis, while PPBs were predominantly transverse with respect to the long axis of the cell supporting a role of POKs in the spatial control of cytokinesis (Müller et al., 2006). TAN and RanGAP1 have been shown to interact with the C-terminal domain of POK1 (Müller et al., 2006; Xu et al., 2008), suggesting that POK1, TAN, and RanGAP1 are part of a functional module required for CDZ identity maintenance. However, the exact nature of this module remains unclear due to the lack of positional information on the POK kinesins.

Here, we provide novel insight into POK function by characterizing a novel *pok2* allele from a mutant screen for *pok1-1* enhancers. In vivo observations of the novel allele combination *pok1-1 pok2-3* revealed lengthy cytokinesis due to a reduced rate of phragmoplast expansion and frequent tilting of late phragmoplasts from their initial orientation. Nevertheless, fusion of the cell plate with the parental wall occurred at seemingly indiscriminate sites resulting in a highly disorganized framework of cell walls, underpinning POKs role in an efficient phragmoplast guidance mechanism and the timely progression through cytokinesis.

Localization studies using a functional yellow fluorescent protein (YFP)-POK1 fusion protein showed that POK1 is recruited to the PPB and remains at the cortex throughout mitosis. Similar to TAN, POK1 initially marks the CDZ and its localization domain narrows down to the CDS prior to cell plate fusion with the parental plasma membrane. POK1 is progressively and dynamically loaded onto the PPB from the cytosol in prophase, while its association with the plasma membrane at the CDZ following PPB degradation appears static. Throughout telophase, the ring-shaped localization narrows from an initial broad band to a sharp string-like pattern that disappears shortly after cell plate fusion. In *pok1 pok2* mutants, the cortical division zone marker TAN disappeared from the CDZ upon entry into metaphase, emphasizing that the POK kinesins function as molecular anchors for other CDZ/CDS identity markers.

RESULTS

POK1 and POK2 Are Required for Guidance of the Phragmoplast toward the Cortical Division Site

Previously, we described two independent *pok1 pok2* double mutant allele combinations, with similar phenotypic defects differing predominantly in their growth rate (Müller et al., 2006). In a sensitized ethyl methanesulfonate (EMS)–induced mutant screen to identify second site mutations in phenotypically wild-type looking *pok1-1* single mutants, we discovered a severe mutant reminiscent of previously characterized *pok1 pok2* double mutants. The novel mutant cosegregated with the *pok1-1* genotype (Supplemental Figures 1A and 1B) and did not complement the *pok1 pok2* double mutant phenotype in test crosses, suggesting that the mutation was located in *POK2*. Sequencing of *POK2* revealed a C-to-T substitution in exon 16, 2197 bp of the coding sequence downstream of the ATG (Figure 1A). The mutation resulted in a premature STOP codon predicted to obliterate about three quarters of the POK2 protein. The allele was designated *pok2-3*. Due to the close linkage of *POK1* and *POK2* on chromosome III, *pok2-3* single mutants were not analyzed.

Overall, the *pok1-1 pok2-3* double mutant displayed an aggravated phenotype compared with the previously described allele combinations *pok1-1 pok2-1* and *pok1-2 pok2-2* (Supplemental Figure 1A; Müller et al., 2006). We reasoned that POK activity was further diminished in these plants and, thus, the novel mutant was used to expand on the in vivo characterization of POK function. The *pok1-1 pok2-3* seedlings displayed shorter and wider roots and hypocotyls and succulent leaves (Figures 1B and 1D). Mature plants were dwarfed similar to weak *ton2* alleles (Kirik et al., 2012; Spinner and Gadeyne et al., 2013), but in contrast to *ton2*, *pok1-1 pok2-3* mutants were fertile (Supplemental Figure 1A). Double *pok1-1 pok2-3* mutants grew significantly shorter roots (Figure 1C) and displayed smaller leaves than *pok1-1 pok2-1* or *pok1-1* (Figure 1D). Although organ formation apparently was not affected, at the cellular level, cell division patterns were dramatically disturbed in *pok1-1 pok2-3* double mutants (Figure 1E, right panel), compared with wild-type and single mutant *pok1-1* root meristems (Figure 1E, left panel).

Previously, immunolocalization of tubulin in root squashes established that phragmoplasts in *pok1 pok2* did not expand in the direction of the former PPB (Müller et al., 2006). To investigate phragmoplast guidance in vivo, the MT reporter line green fluorescent protein (GFP)-MBD was introgressed into the *pok1-1 pok2-3* double mutants. As in *pok1-1 pok2-1* and *pok1-2 pok2-2* (Müller et al., 2006), PPB, spindles, and phragmoplasts formed normally in the *pok1-1 pok2-3* double mutant root meristem cells (Supplemental Figure 2). Time-lapse recordings of phragmoplast expansion, encompassing the stage of spindle-to-phragmoplast transition until completion of phragmoplast disassembly, revealed that phragmoplasts frequently tilted (Figures 2A, 2B, and 2D; Supplemental Movies 1 and 2 and Supplemental Figures 3A and 3B) and that the duration of cytokinesis was prolonged in *pok1-1 pok2-3* double mutants (Figure 2C). While in the wild type cytokinesis lasted 37 min $\pm$ 11 min (n = 24) on average, in the double mutant, cytokinesis lasted on average 57 min $\pm$ 24 min (n = 17, *P < 0.05) (Figure 2C). In wild-type meristems, optical sections through phragmoplasts typically display the transverse double layer of

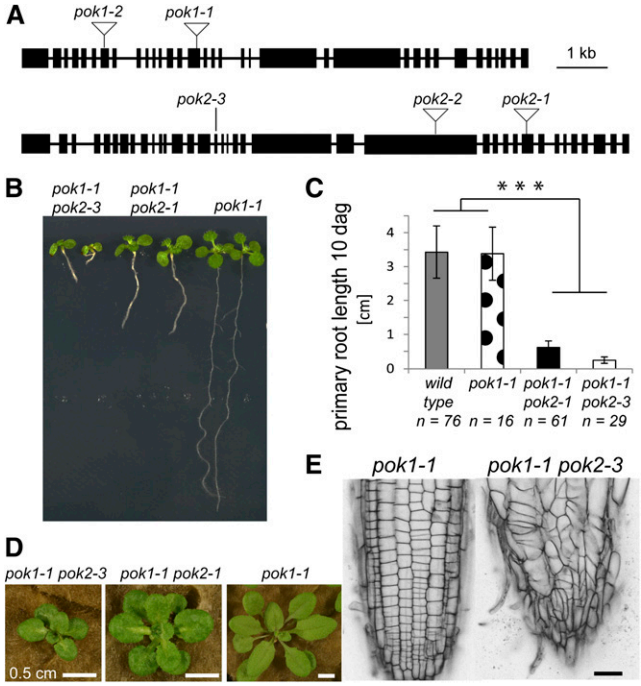

Figure 1. Mutant Alleles and Mutant Phenotypes.

(A) Schematic representation of *POK1* and *POK2* gene structure and position of mutations. SALK-T-DNA insertions in alleles *pok1-1* (exon 15), *pok1*-2 (exon 7), *pok2-1* (exon 28), and *pok2-2* (exon 23) are indicated by triangles. The ethyl methanesulfonate–induced nonsense mutation in allele *pok2-3* is a C-to-T substitution (exon 16, at position 3845 bp), causing a premature stop at amino acid 733 (Gln to *). Bars indicate exons.
(B) Seedling phenotypes of (right to left) the *pok1-1* single mutant, *pok1-1 pok2-1* double mutant, and *pok1-1 pok2-3* double mutant.
(C) Comparison of average primary root length 10 d after germination (dag). Gray bar indicates the wild type (3.4 cm ± 0.8), dotted bar indicates *pok1-1* (3.4 cm ± 0.8), black bar indicates *pok1-1 pok2-1* (0.6 cm ± 0.2), and gray bar indicates *pok1-1 pok2-3* (0.25 cm ± 0.09). The average root length of *pok1-1 pok2-1* and *pok1-1 pok2-3* is significantly (***P << 0.005, Student's *t* test) shorter than in the wild type and *pok1-1*. Number of samples is indicated. Error bars indicate ±SD.
(D) Comparison of rosettes of 3-week-old *pok1-1* single mutant, *pok1-1 pok2-3* double mutant, and *pok1-1 pok2-1* double mutant plants.
(E) Root meristems, stained with propidium iodide to visualize cell walls. Whereas the *pok1-1* single mutant (left) shows a regular cell pattern of the root cell files, the *pok1-1 pok2-3* double mutant (right) cell pattern is completely disorganized.
Bar = 0.5 cm in **(B)** and 20 μm in **(E)**.
[See online article for color version of this figure.]

antiparallel MTs connecting in the midzone (Figure 2A), which expands laterally throughout cytokinesis. In the wild type, periclinal root divisions, allowing a view of the phragmoplast torus/ring while it expands, occur with a very low frequency close to the root apical meristem as the *Arabidopsis* root contains a single layer of epidermal, cortical, and endodermal tissue. Remarkably, 23% of cytokinetic cells in *pok1-1 pok2-3* double mutants displayed the phragmoplast ring view (Figure 2D), while only 2.4% of cytokinetic cells in the wild type exhibited the phragmoplast ring, in agreement with altered division plane orientations in *pok1-1 pok2-3*.

To determine whether the rate of phragmoplast expansion contributed to the prolonged cytokinesis in the *pok1-1 pok2-3* double mutant, we compared the rate of phragmoplast expansion using kymograph analysis (Figures 2E and 2F). Regardless of the genotype, most phragmoplasts displayed an expansion asymmetry as reflected by varying inclines of the kymograph (Figure 2F, left panel). This demonstrated that lateral expansion of the phragmoplast did not occur at a steady velocity, also indicated by the high SD (Figure 2G). Nevertheless, in *pok1-1 pok2-3* double mutants, the average expansion rate was moderately, but significantly reduced (0.18 ± 0.09 μm/min; *P < 0.02, *n* = 22) compared with the wild type (0.21 ± 0.09 μm/min; *n* = 43) (Figure 2G), suggesting that slowing of the expansion rate in the double mutant contributes to the observed prolonged cytokinesis together with the frequent tilting of the phragmoplast.

POK1 Interacts with TAN through Its C-Terminal Domain and Is Required for TAN Maintenance at the CDZ but Not for Its Recruitment

As previously reported, TAN maintenance at the CDZ requires POK function, while recruitment to the PPB occurred, although inefficient, in *pok1 pok2* mutants (Walker et al., 2007), in agreement with two distinct TAN protein domains mediating TAN recruitment to the CDZ before and after PPB disassembly (Rasmussen et al., 2011). To clarify the role of POKs in TAN recruitment, we analyzed TAN localization in the severe *pok1-1 pok2-3* allele combination (Figure 3). In the wild type, the majority of cells displaying either the PPB (95%, *n* = 19 cells), pro-spindle (100%, *n* = 6 cells), spindle (92%, *n* = 12 cells), or phragmoplast (98%, *n* = 43 cells) also contained associated cortical TAN rings (Figures 3A to 3D). In contrast, the TAN recruitment in cells with PPBs (55%, *n* = 11 cells) seemed less efficient or delayed, but not abolished in *pok1-1 pok2-3* double mutants, consistent with results from previous studies. Interestingly, the cortical association of TAN in cells containing pro-spindles was high (89%, *n* = 9 cells; Figure 3E), suggesting that POK function was not critically required for TAN localization at prophase. However, the percentage of TAN rings in cells displaying spindles in metaphase dropped to 19% (*n* = 16 cells; Figures 3F, 3G, and 3I), indicating that binding of POK1 and TAN becomes essential during this cell cycle stage. Moreover, TAN rings were entirely absent from cells with phragmoplasts (0%, *n* = 18 cells; Figure 3H) in *pok1 pok2* double mutants. This result further supports the partial POK dependence of TAN at the PPB and the essential POK1-dependent maintenance of TAN following prophase. In addition, we showed in planta interaction of nYFP-POK1$_{1683-2066}$ and cYFP-TAN in *Arabidopsis* protoplasts using bimolecular fluorescent complementation (BiFC) (Figures 3J and 3K), supporting that interaction between TAN and POK1 mediates TAN maintenance at the CDZ. In contrast to control experiments (Figures 3L to 3N), strong expressing protoplasts displayed a filamentous YFP pattern reminiscent of cortical MTs (Figure 3O), suggesting that stabilization of POK1 and TAN interaction increases their capacity for MT binding

POK1 Localizes to the Cortical Division Zone

We analyzed the localization pattern of a functional YFP-POK1 fusion (Supplemental Figures 1C and 1D) in 4- to 6-d-old wild-type

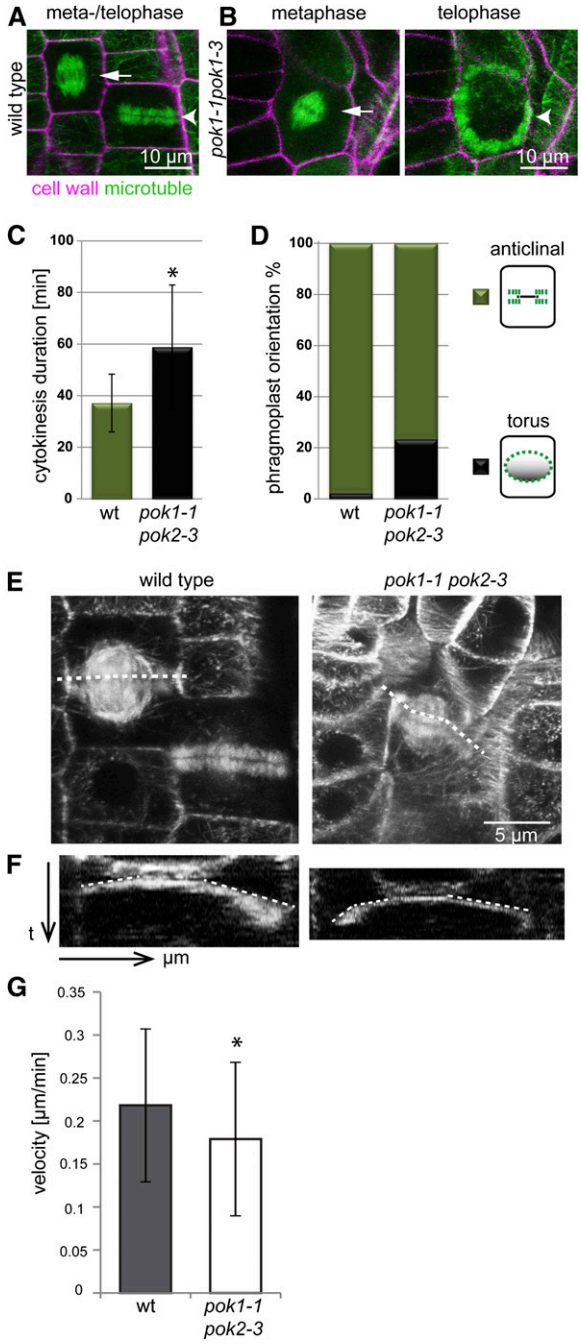

Figure 2. Duration of Cytokinesis and Orientation of Phragmoplast Expansion.

Orientation of spindles (arrows) and phragmoplasts (arrowheads).

(A) A wild-type spindle and phragmoplast in a characteristic anticlinal orientation, with the phragmoplast expanding toward the lateral cell walls, perpendicular to the optical plane.

(B) A *pok1-1 pok2-3* mutant cell in metaphase (spindle) and the same cell during cytokinesis (phragmoplast). The spindle is slightly tilted. The phragmoplast expands in an oblique or periclinal orientation, thus presenting its torus.

(C) The duration of phragmoplast expansion is significantly extended in *pok1-1 pok2-3* mutants (58 min ± 24 min, *P > 0.01, *n* = 17) compared with the wild type (37 min ± 11 min, *n* = 24).

seedlings (Figure 4; Supplemental Figure 3). Only a subset of meristematic cells displayed a fluorescent YFP-POK1 signal, suggesting cell cycle–controlled expression or degradation of POK1. POK1-expressing cells displayed distinct fluorescent patterns of broad bands, sharp bands, or pairs of focused spots (Figure 4A) in single optical sections. Three-dimensional reconstruction of confocal image stacks revealed that YFP-POK1 formed continuous rings at the cell cortex.

To correlate the distinct YFP-POK1 rings with the corresponding cell cycle stages, we coexpressed YFP-POK1 and the MT reporter red fluorescent protein (RFP)-MBD. In root and leaf meristems, YFP-POK1 rings were associated with mitotic cells exhibiting PPBs, spindles, and phragmoplasts (Figure 4B; Supplemental Figures 4A and 4B). The observed YFP-POK1 patterns were reminiscent of the ring-shaped localization observed for the two POK1 interactors TAN and RanGAP1, which both colocalize with the PPB and continuously mark the CDZ throughout mitosis (Walker et al., 2007; Xu et al., 2008).

The short C-terminal fragment $POK1_{1683-2066}$ shown to be sufficient to bind TAN (Müller et al., 2006; this study) and RanGAP1 (Xu et al., 2008) fused to YFP (*Pro35S*:YFP-$POK1_{1683-2066}$; Figure 4C) accumulated mainly in aggregates in *Arabidopsis* root meristem cells (Supplemental Figure 4C), constraining detection of a potential cortex localization.

Since $POK1_{1683-2066}$ showed substantial aggregation, we tested whether aggregation could be prevented by expressing longer fluorophore-tagged constructs of the POK1 C-term (*Pro35S:GFP-*$POK1_{1213-2066}$ and *ProTP1:dTom-*$POK1_{1265-2066}$; Supplemental Figure 4D). Both fusion proteins displayed a cell cycle–dependent subcellular localization pattern similar to the full-length YFP-POK1 and vastly diminished aggregation (Supplemental Figures 4E and 4F).

POK1 Cortical Recruitment Shows Cell Phase–Dependent Dynamicity

To further characterize POK1 cortical recruitment, fluorescence recovery after photobleaching (FRAP) analysis was performed

(D) In the wild type (*n* = 49), 97.96% of the observed phragmoplasts displayed anticlinal orientation and only 2.04% were oriented with their torus parallel to the optical plane. In contrast, in *pok1-1 pok2-3* mutants (*n* = 43), the proportion of phragmoplasts presenting the torus (ring view) rises to 23.26%.

(E) Projection of a time series throughout mitosis for wild type (45 min, 19 image stacks) and *pok1-1 pok2-3* mutants (60 min, 25 images). At 2.5-min intervals, image stacks were taken from mitotic cells at 1-µm z-intervals throughout the duration of mitosis. Maximum z-projections of each time point were projected for the depicted images. The white dotted lines indicate the selection for the kymograph analysis.

(F) Space-time plots (kymographs) of respective phragmoplasts depicted in **(E)**. The x-coordinate depicts the distance in micrometers. The y-coordinate indicates the time t. The kymograph plug-in in ImageJ was used to create kymographs and calculate the velocity of phragmoplast expansion. The slopes of the kymograph (contrast edge, selection is indicated by white dotted lines) are proportional to the velocity. In these examples, the two halves of the phragmoplasts expanded at different velocities. In addition, in one half the velocity decreased, indicated by the change in slope (two-phase expansion).

(G) The average velocity of phragmoplast expansion is significantly reduced in *pok1-1 pok2-3* mutants (0.18 ± 0.09 µm/min; P < 0.02, *n* = 22, Student's *t* test), compared with the expansion rate in the wild type (0.21 ± 0.09 µm/min; *n* = 43). Error bars indicate ±SD. Cell walls are stained with propidium iodide. Microtubules are visualized by GFP-MBD.

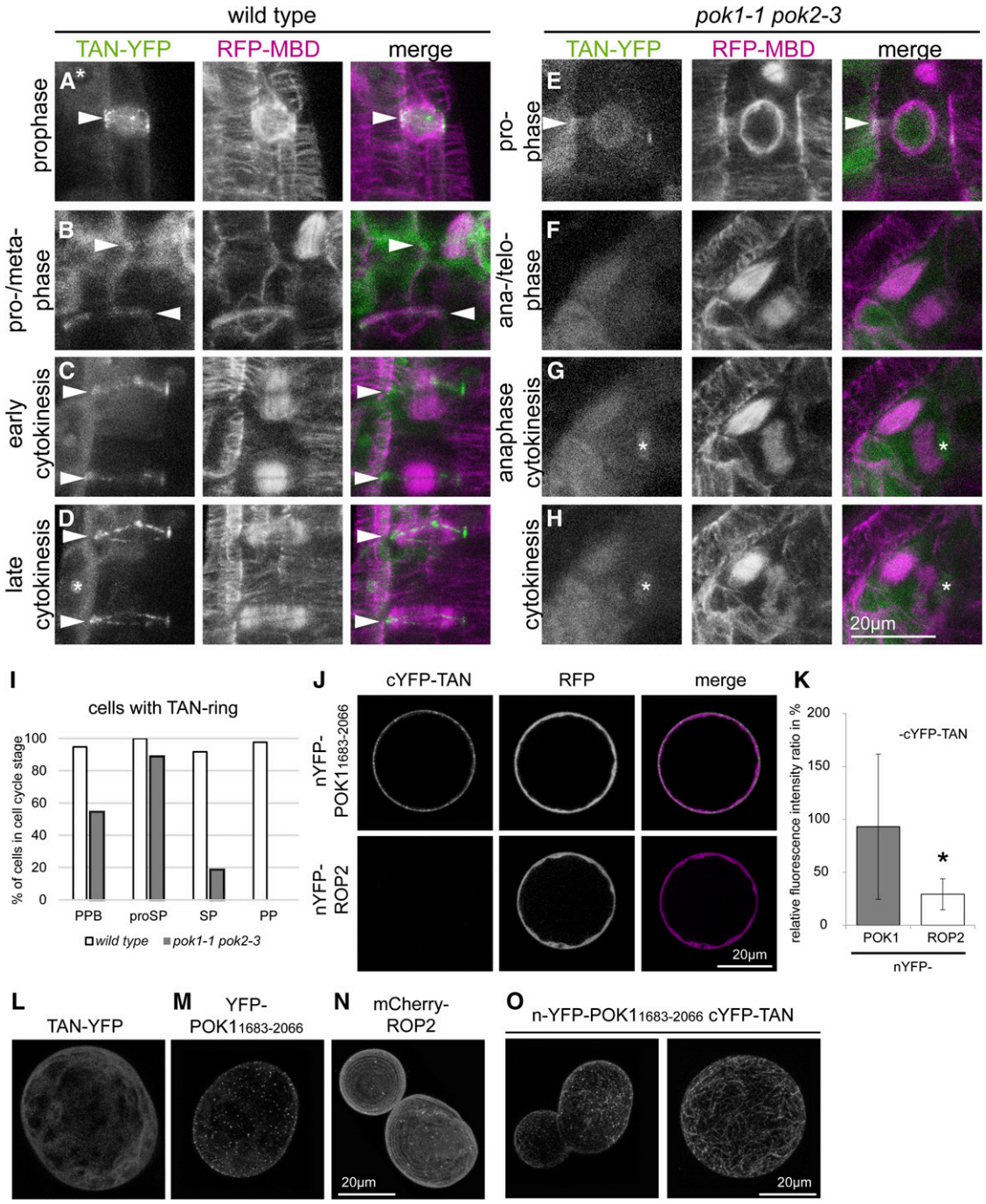

Figure 3. Loss of POK-Dependent TAN Localization at the Cortical Division Zone Correlates with PPB Disassembly.

(A) to **(D)** TAN-YFP is recruited to the preprophase band in the wild type **(A)** and *pok1-1 pok2-3* double mutants **(E)**. In the wild type, TAN-YFP rings coexist with the preprophase band (**[A]** and **[B]**), pro-spindle **(B)**, spindle **(B)**, and early late phragmoplasts (**[C]** and **[D]**).

(E) Cell with pro-spindle displaying the TAN-YFP ring.

(F) The spindle in the metaphase cell is not associated with cortical TAN-YFP nor does the signal reappear during cytokinesis (**[F]** to **[H]** represent a time series). Images are z-projections of a varying number of images taken at 1-μm intervals. TAN-YFP rings are indicated by arrowheads. The nuclear localization of YFP-TAN is indicated by an asterisk. Bar = 10 μm.

(I) Presence of TAN-YFP rings during the cell cycle in wild type and *pok1-1 pok2-3* mutants.

(J) to **(K)** Interaction of TAN and the POK1 C terminus, as determined by BiFC.

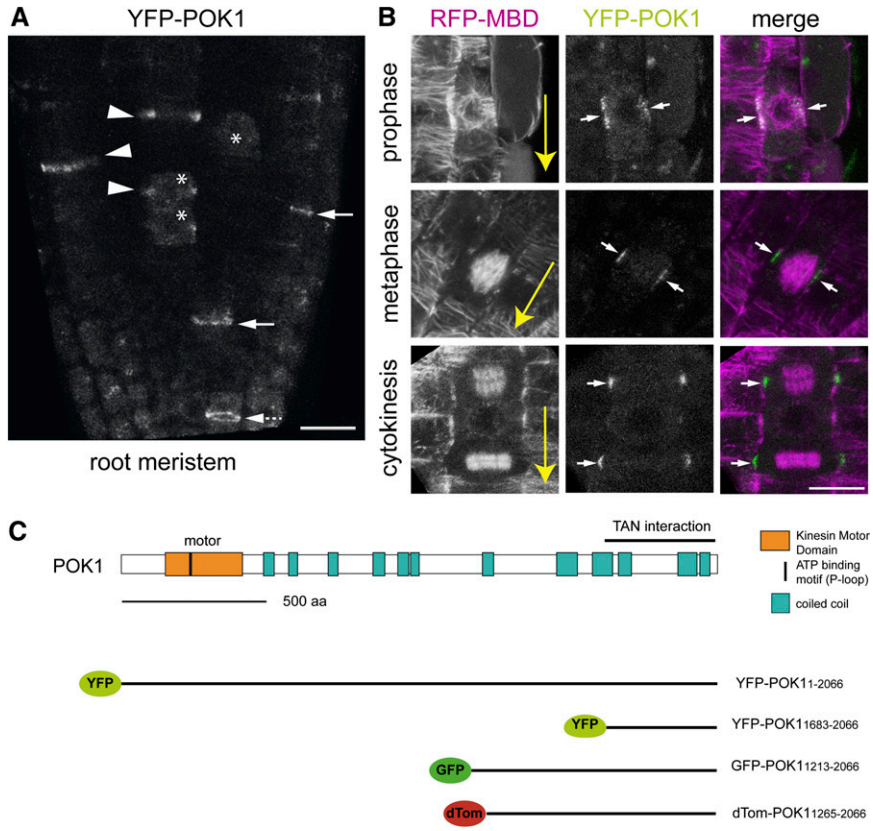

Figure 4. POK1 Localizes at the Cortical Division Zone/Site.

(A) Maximum z-projection of a root meristem expressing YFP-POK1. In cross sections, YFP-POK1 localizes as broad bands or dots (arrowheads) and sharp bands (arrows). Occasionally, YFP-POK1 rings are visible (arrow with dotted shaft). Some cells accumulate cytoplasmic YFP-POK1 (asterisk).
(B) Coexpression of RFP-MBD and YFP-POK1 in different cell cycle stages in the root. YFP-POK1 colocalizes with the PPB in prophase and remains at the cell cortex throughout mitosis. Large yellow arrows indicate the longitudinal root axis.
(C) POK1 domain organization as indicated in the legend and overview of fluorescent protein fusions used for localization studies. The $POK1_{1683-2066}$ fragment corresponds to the TAN-interacting fragment used in the BiFC experiment (Figures 3J and 3K).
Bar = 20 μm in **(A)** and 10 μm in **(B)**.

(Figures 5 and 6). In the *Arabidopsis* root meristem, epidermis cells in pro- and metaphase were selected based on the presence or absence of condensed nuclei in bright field. In transverse sections, YFP-POK1 localized to both lateral cell sides (Figures 5A to 5D). YFP-POK1 was specifically bleached at one side of the confocal section and migration of fluorescent signal into the bleached region was subsequently monitored. In prophase cells, fluorescence clearly recovered during the observation period (Figures 5A, 5C, and 5E). By contrast, metaphase YFP-POK1 fluorescence hardly recovered (Figures 5B, 5D, and

Figure 3. (continued).

(J) Confocal images of an *Arabidopsis* protoplast coexpressing nYFP-$POK1_{1683-2066}$ and cYFP-TAN or nYFP-ROP2 and cYFP-TAN as negative controls. YFP fluorescence was specifically detected upon complementation of the fluorophore due to TAN and $POK1_{1683-2066}$ interaction in contrast to the control experiment. RFP, expressed from the same plasmid, was used as an internal control.
(K) Quantification of mean YFP fluorescence expressed as a ratio of mean RFP fluorescence. Data are means ± SD of 26 protoplasts per construct, each representing independent transformation events. The YFP/RFP ratio is significantly different (*$P < 0.001$, Student's *t* test) between TAN/$POK1_{1683-2066}$ (interaction) and TAN/ROP2 (no interaction).
(L) to **(N)** Localization of controls in protoplasts as indicated. Images are maximum z-projections of image stacks taken at 1-μm z-intervals. Bar = 20 μm.
(L) Cytoplasmic localization upon expression of *Pro35S:TAN-YFP*.
(M) Expression of *Pro35S:YFP-POK1*$_{1613-2066}$ leads to punctate YFP signal in the plasma membrane similar to what is observed in *Arabidopsis* root meristem cells.
(N) Expression of *pUB10:mCherry-ROP2*.
(O) Examples of protoplasts coexpressing nYFP-$POK1_{1683-2066}$ and c-YFP-TAN. Images are maximum z-projections of image stacks taken at 1-μm z-intervals. Bar = 20 μm.

5E), indicating a more dynamic YFP-POK1 recruitment or dispersal mechanism during prophase and a fairly static maintenance mechanism during subsequent cell cycle phases. The POK1 C-terminal fragment GFP-POK1$_{1213-2066}$ in BY-2 cells displayed differential dynamicity in FRAP experiments similar to YFP-POK1 in *Arabidopsis* (Figures 6A to 6D). Also in prophase BY-2 cells, fluorescent signal recovered, although at a longer half-time (Figure 6D) than YFP-POK1 (Figure 5E), while BY-2 metaphase cells displayed sluggish GFP-POK1$_{1213-2066}$ signal recovery similar to YFP-POK1. Due to the superior imaging accessibility, we clarified whether the initial recruitment of POK1 to the CDZ requires MTs, using BY-2 cells. Prophase cells expressing *ProS35:POK1$_{1213-2066}$-GFP* were treated with oryzalin and subjected to FRAP analysis. The oryzalin treatment completely abolished fluorescence recovery to the CDZ at prophase following photobleaching (n = 6) (Figures 6E to 6L), suggesting the MT-dependent recruitment of POK1$_{1213-2066}$-GFP.

In *Arabidopsis*, a proportion of mitotic cells accumulated full-length YFP-POK1 signal in the cytoplasm, both in the absence and presence of YFP-POK1 cortical rings (Figure 4A, asterisk). We determined the proportion of cells containing cytoplasmic YFP-POK1 and/or YFP-POK1 at the CDZ for each cell cycle stage (Supplemental Figure 4A). In the presence of PPBs, YFP-POK1 accumulates in the cytoplasm and progressively associates with the PPB and the CDZ in pro-metaphase, suggesting that YFP-POK1 is dynamically recruited to the CDZ. From metaphase until the termination of cytokinesis, the majority of YFP-POK1 was found to be associated with the CDZ. Taken together, our data suggest a cell cycle–dependent relocalization from cytoplasmic to cortical, CDZ/CDS resident YFP-POK1.

Similar to TAN (Walker et al., 2007; Rasmussen et al., 2011; Supplemental Figures 4B and 4C) and RanGAP1 (Xu et al., 2008), the ring-shaped localization of POK1 narrowed during cytokinesis in BY-2 cells (Figures 6B and 6C; Supplemental Figures 5D and 5E) and *Arabidopsis* (Figures 5A and 5B) in a cell cycle progression-dependent manner. While the sharp punctate signal corresponds to the site of cell plate fusion, the CDS, the broad POK1 signal corresponded to the wider CDZ.

YFP-POK1 CDZ/CDS Localization Is Independent of Microtubules

To analyze the microtubule dependency of the subcellular YFP-POK1 localization, seedlings coexpressing YFP-POK1 and RFP-MBD were treated with the MT polymerization inhibitor oryzalin. The effect of oryzalin was visualized by the depolymerization of RFP-MBD-labeled MTs. While mitotic MT arrays disappeared upon oryzalin treatment (Figures 5F and 5H), YFP rings associated with cells containing PPBs (Figure 5G), spindles, or phragmoplasts prior to oryzalin treatment were still present after MT depolymerization (Figures 5G and 5I, Table 1). In two instances, the PPB was not associated with a YFP-POK1 ring (Table 1, n = 10 PPBs), which is consistent with the progressive recruitment of POK1 to the CDZ during prophase. In addition to the YFP-POK1 rings present in cells with phragmoplasts (n = 15), five more (sharp) YFP-POK1 rings associated with recently synthesized cell walls (Table 1), which we also frequently observed in untreated cells. Maintenance of cortical POK1 upon oryzalin treatment demonstrates the MT-independent maintenance of CDZ-resident YFP-POK1.

Taken together, these results suggest that dynamic POK1 is continuously recruited to the CDZ in a microtubule-dependent manner during prophase, most likely from a cytoplasmic pool that is depleted prior to metaphase. Upon PPB disassembly, POK1 becomes immobilized and its localization subsequently narrows as mitosis progresses likely involving a self-associating mechanism. Independently of POK function, TAN and RanGAP1 arrive at the PPB where they become tethered by a POK-dependent mechanism. Together, these proteins constitute a modular hub to maintain the positional information of the division plane and to guide the phragmoplast during cytokinesis.

DISCUSSION

The correlation between the orientation of the PPB and the direction of phragmoplast expansion is a long-standing dogma in plant cell biology (Gunning and Wick, 1985). Cell biological studies on cell cultures and the use of a variety of chemicals interfering with cytoskeletal organization/dynamics as well as mutant analysis demonstrated the causal relation of PPB position and guidance of the phragmoplast toward the site specified by the PPB (Torres-Ruiz and Jürgens, 1994; Traas et al., 1995; Smith et al., 1996; Camilleri et al., 2002; Sano et al., 2005). Yet, the molecular mechanisms involved remain poorly characterized. In contrast, upstream processes such as auxin-dependent transcriptional control of local cell divisions, essential for embryonic patterning, are intensively studied (reviewed in Lau et al., 2012). For instance, the ectopic expression of the bHLH transcription factor TMO5 is sufficient to induce periclinal divisions (De Rybel et al., 2013).

The proteins TAN and the POK kinesin-12 proteins were implicated in phragmoplast guidance due to the mispositioning of cell walls in the corresponding mutants with respect to the former PPB position (Smith et al., 1996; Müller et al., 2006), but how these proteins functionally interacted was unclear due to the lack of subcellular data regarding the POK kinesins. Our in vivo analysis confirmed the frequent mismatch of PPB and phragmoplast orientation in dividing *pok1 pok2* cells, showing that the POK kinesins function downstream of PPB formation and division plane determination. In contrast, in mutant alleles of microtubule-associated proteins such as CLASP (Ambrose et al., 2007; Kirik et al., 2007), PP2A subunit mutants (Spinner and Gadeyne et al., 2013) and the putative membrane protein SABRE (Pietra et al., 2013), oblique cell walls and misguidance of the phragmoplast are a consequence of mispositioning of the PPB or lack thereof and, thus, these proteins act upstream of the POKs.

Consistent with phragmoplast expansion in BY-2 cells (Buschmann et al., 2010), we determined distinct expansion velocities for the left and right edge of wild-type and *pok1-1 pok2-3* phragmoplasts. The rate of phragmoplast expansion was diminished in *pok1-1 pok2-3* cytokinesis, but could not solely account for the difference with respect to wild-type cytokinesis duration. Tilting of the *pok1-1 pok2-3* phragmoplast contributes to the extended duration of *pok1-1 pok2-3* cytokinesis as well, since the tilted cell plate apparently does not follow the shortest distance rule (Rasmussen et al., 2013) in the

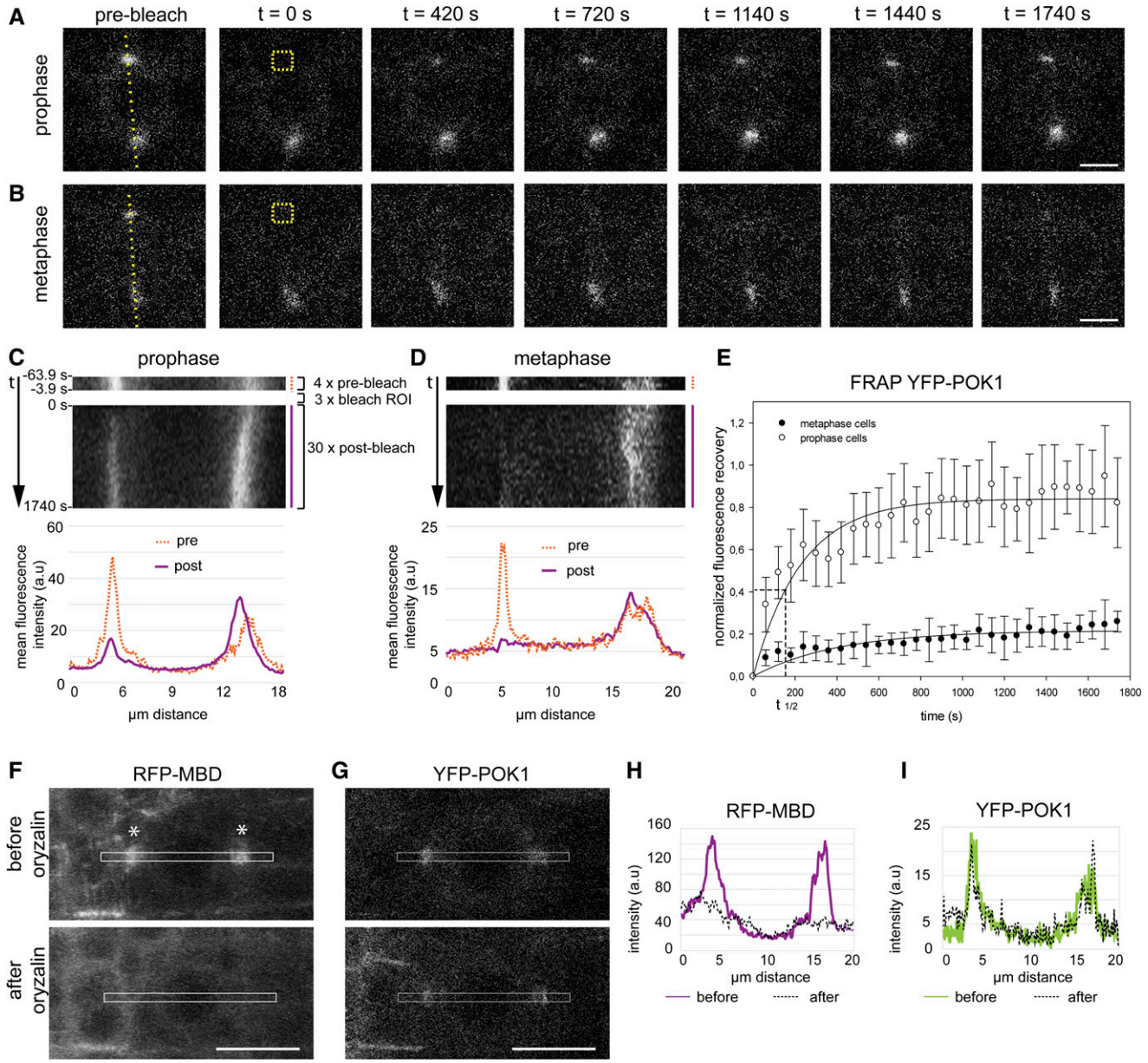

Figure 5. Differential POK1 Dynamicity during Mitosis.

(A) and **(B)** FRAP analysis of YFP-POK1. Representative time lapse of mitotic cells in the *Arabidopsis* root meristem. Transverse sections of **(A)** prophase and **(B)** metaphase cells recorded at different time points before (prebleach) and after photobleaching. Bleach regions are indicated by a dashed square (ROI) in first postbleach images (t = 0 s). Bar = 5 μm.

(C) and **(D)** Kymographs of prebleach and postbleach time series corresponding to the dashed line selection as indicated in the prebleach images of **(A)** and **(B)**. Prebleach kymograph (orange dashed line) of four prebleach images and postbleach kymograph of 30 postbleach images (magenta solid line) and corresponding profile plots are depicted. Profile plots show mean fluorescence intensities from the prebleach (orange dashed line) and postbleach (magenta solid line) kymographs, respectively. Note the recovery of YFP signal in prophase.

(E) An average of independent FRAP experiments is plotted to fit a single exponential curve with rise to a maximum (y = a*(1-exp(-b*x))). In prophase cells (n = 10), the YFP-POK1 signal recovers after photobleaching with a half-time ($t_{1/2}$) of 154 s, while there is hardly any fluorescence recovery in metaphase cells (n = 6). Error bars indicate ±SD.

(F) to **(I)** POK1 localization at the cortical division zone is independent of MTs. Maximum z-projections of an *Arabidopsis* root meristem prophase cell coexpressing the MT reporter RFP-MBD **(F)** and YFP-POK1 **(G)** before and after treatment with 10 μM oryzalin. The PPB is indicated by asterisks.

(F) and **(G)** Lower panels were recorded 15 min after oryzalin incubation and correspond to the cell in the upper panels. Due to MT depolymerization, the RFP-MBD reporter localization becomes cytosolic, while the YFP-POK1 signal remains present at the CDZ. Bar = 10 μm.

(H) and **(I)** Fluorescence intensity profile plots from a rectangular selection in **(F)** and **(G)** depicting RFP-MBD **(H)** signal distribution before oryzalin treatment (continuous, magenta line) and after oryzalin treatment (dashed, black line) and YFP-POK1 **(I)** signal distribution before (continuous, green line) and after (dashed, black line) oryzalin treatment. Note that the RFP-MBD peaks disappear after oryzalin treatment, while the YFP-POK1 peaks remain.

[See online article for color version of this figure.]

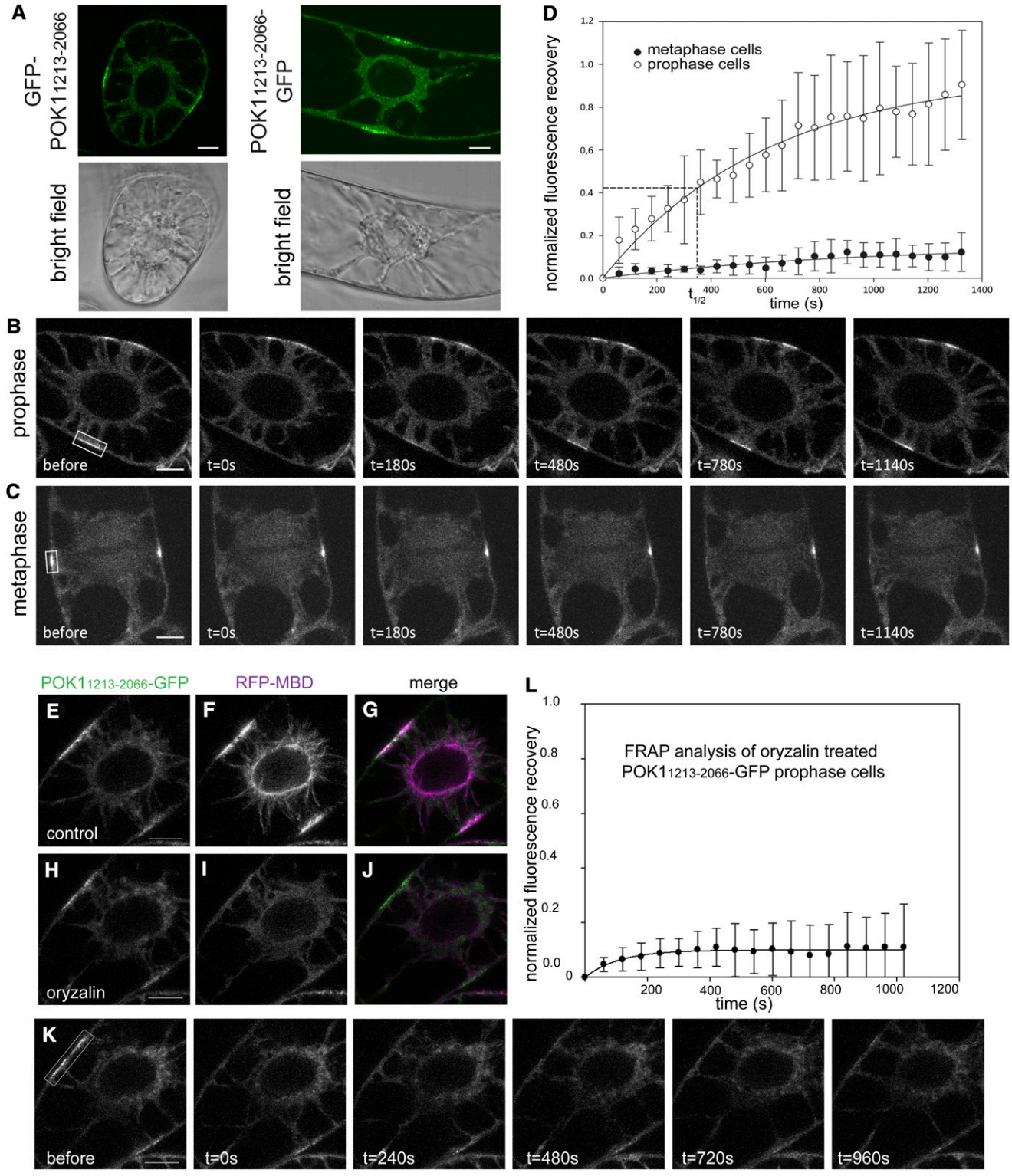

Figure 6. Changes of POK1 Dynamicity during Mitosis.

(A) A tobacco BY-2 cell expressing *Pro35S:GFP-POK1*$_{1213-2066}$ and *Pro35S:POK1*$_{1213-2066}$-GFP and the corresponding bright-field image. Bar = 10 μm.
(B) to **(D)** FRAP analysis of GFP-POK1C.
(B) Representative time lapse of a prophase BY-2 cell after photobleaching of GFP-POK1C at the PPB (white box indicates the bleached area).

Table 1. Association of YFP-POK1 with the Cortical Division Site Is Independent of Microtubules

	RFP-MBD			YFP-POK1		
n = 8 roots	PPB	Spindle	Phragmoplast	PPB	Spindle	Phragmoplast
Before oryzalin	10	5	15	8	4	20
After oryzalin	0	0	0	8	4	16

While microtubules disassembled, YFP-POK1 signal was not affected upon oryzalin treatment.

absence of POK-dependent phragmoplast guidance. The postulated direct correlation of cytokinesis duration and cell size (Gorst et al., 1986) is consistent with this assumption.

The cell cycle–dependent association of POK1 with the CDZ/CDS closely resembles the localization of CDZ/CDS identity markers TAN and RanGAP1 (Walker et al., 2007; Xu et al., 2008). Interaction of $POK1_{1683-2066}$ with TAN as determined by BiFC (Figure 3) and the phenotype similarity of the maize mutant *tan* (Smith et al., 1996; Cleary and Smith, 1998) and the *pok1 pok2* double mutant in *Arabidopsis* further support a joint function of POK1 and TAN in the phragmoplast guidance mechanism.

POK1, TAN (Walker et al., 2007), and RanGAP1 (Xu et al., 2008) share the feature of narrowing from a broad toward a sharp ring during cytokinesis, suggesting that the proteins are coregulated and/or act in a complex. POK1 seems to be particularly important for CDZ identity maintenance throughout mitosis, since both TAN (this study; Walker et al., 2007) and RanGAP1 (Xu et al., 2008) fail to remain present in *pok1 pok2* double mutants upon the metaphase/anaphase transition. Thus, the narrowing of TAN (Walker et al., 2007) and RanGAP1 (Xu et al., 2008) might reflect the narrowing of POK1 at the CDZ. With respect to TAN and RanGAP1 maintenance, POK1 provides a scaffolding function to retain CDZ resident proteins, thereby sustaining CDZ identity. Although the C-terminal $POK1_{1683-2066}$ is sufficient for TAN interaction, GFP-$POK1_{1683-2066}$ localization at the CDZ could not be unambiguously confirmed, in contrast to GFP-$POK1_{1213-2066}$, indicating that the necessary additional domain for efficient POK1 targeting to the PPB and CDZ lies directly upstream of $POK1_{1683-2066}$. With few exceptions, most kinesin class proteins act as homo- or heterodimers (Endow et al., 2010), mediated by multiple coiled coil domains, which are also predicted for POK1 and POK2 C termini (Figure 4C). Thus, the POK1C-terminal fusion proteins might associate with the PPB/CDZ through self-dimerization or with endogenous full-length POKs. Alternatively, the POK1C-terminal might be necessary and sufficient to recruit POK1 to the PPB and CDZ via interactions with yet unknown membrane-anchored binding partners.

Although the localization of POK2 was not directly investigated here, the rescue ability of the full-length YFP-POK1 fusion protein and the absence of aberrant single mutant phenotypes indicate functional redundancy of POK1 and POK2 and therefore also similarity in localization. In light of functional redundancy of POK1 and POK2, the aggravated phenotype of the novel *pok1-1 pok2-3* allele combination can be explained by the fact that some POK2 activity might still be present in previously described double mutants.

Genetic evidence suggests that TAN arrives at the PPB independently of POK1; however, both POK1 and TAN1 (Walker et al., 2007) recruitment to the PPB require an intact microtubule cytoskeleton. To clarify the sequence of independent recruitment events at the PPB, time-resolved in vivo colocalization studies of POK1, TAN, and RanGAP1 proteins would prove useful, since genetic analysis in *Arabidopsis* is hampered by the lack of clear *tan* loss-of-function alleles as well as the pleiotropic phenotypes of *ran gap* double knockdown mutants (Xu et al., 2008) and gametophytic lethality of *ran gap* double knockout mutants (Rodrigo-Peiris et al., 2011), respectively.

Based on homology of the motor domains, POK1 clusters with kinesin-12 class proteins, predicted to display MT plus end directed motility (Lee and Liu, 2004; Müller et al., 2006; Lipka and Müller, 2012). Although POK1 motor activity has not been investigated, given its localization at the plasma membrane, it potentially contributes to the phragmoplast guidance mechanism by directly binding to peripheral phragmoplast MTs and

Figure 6. (continued).

(C) Representative time lapse of a metaphase BY-2 cell after photobleaching the GFP-POK1 C terminus at the CDZ (indicated by white box).

(D) Graph representing FRAP data for prophase and metaphase BY-2 cells overexpressing GFP-$POK1_{1213-2066}$. In prophase cells, the GFP-POK1 signal recovers slowly after photobleaching with a half-time ($t_{1/2}$) of 362 s, while there is hardly any fluorescence recovery in metaphase cells. An average of independent FRAP experiments is plotted to fit a single exponential curve with rise to a maximum (y = a*(1-exp(-b*x))) (prophase cells: *n* = 4; metaphase cells: *n* = 7). Error bars indicate ±SD.

(E) to **(L)** Recruitment of POK1C-GFP requires MTs, whereas PPB-localized POK1C-GFP statically associates with the CDZ independently of MTs in BY-2 cells.

(E) to **(J)** Representative dividing BY-2 cell coexpressing the *Pro35S:RFP-MBD* MT marker and *Pro35S:$POK1_{1213-2066}$-GFP.*

(E) to **(G)** POK1C-GFP colocalizes with the preprophase band (**[E]**, POK1C-GFP; **[F]**, RFP-MBD; **[G]**, merged image).

(H) to **(J)** Upon oryzalin treatment, MTs depolymerize while POK1C-GFP remains associated with the CDZ (**[H]**, POK1C-GFP; **[I]**, RFP-MBD; **[J]**, merged image).

(K) Representative time lapse of POK1C-GFP FRAP performed on oryzalin-treated BY-2 cells in **(E)**. In the absence of MTs, POK1C-GFP fluorescence did not recover at the bleached CDZ region. The bleached area is indicated by a white box.

(L) Graph representing the FRAP experiments performed on oryzalin-treated prophase BY-2 cells coexpressing the *Pro35S:RFP-MBD* microtubule marker and *Pro35S:$POK1_{1213-2066}$-GFP* (*n* = 6). GFP fluorescence did not recover at the CDZ upon MT depolymerization. Bar = 10 μm; error bars indicate ±SD. [See online article for color version of this figure.]

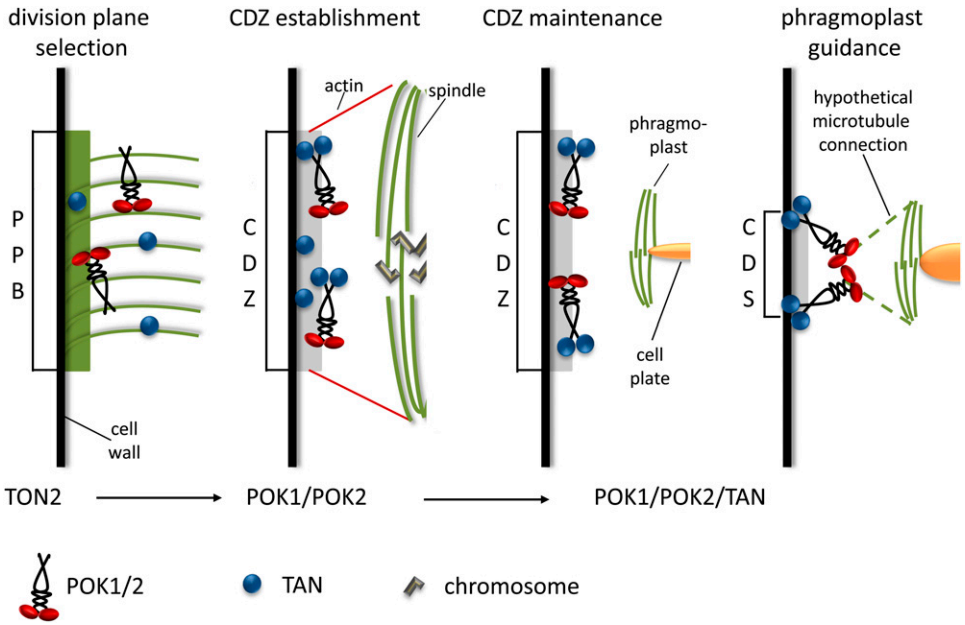

Figure 7. Schematic Representation of Cell Cycle–Dependent Localization and Function of POK1.

In prophase cells, POK1 and TAN are independently recruited to the TONNEAU2-dependent PPB. Upon metaphase, POK1 becomes immobilized at the CDZ, and at the same time, TAN is tethered to the CDZ in a POK1/POK2-dependent manner, likely through direct binding to the C terminus of POK1. Toward the end of cytokinesis, POK1 and TAN localization narrows to the exact site of cell plate anchoring at the parental wall, the CDS, via a yet unknown mechanism. Dashed line indicates likely transient microtubules connecting the phragmoplast with the CDS at late cytokinesis (Supplemental Figure 6).
[See online article for color version of this figure.]

exerting a motor activity–related force. Alternatively, POK, together with TAN, might simply function to stabilize outreaching MTs. Indeed, TAN is a highly basic protein that cosediments with MTs in vitro (Smith et al., 2001), showing that it has MT binding capacities. In this hypothesis, the motor activity required for orienting the phragmoplast might be delivered by phragmoplast-associated kinesins. Stabilization of the $POK1_{1683-2066}$ and TAN protein complex by reconstitution of YFP in the BiFC experiment drew the complex to filamentous cellular structures, closely resembling MTs, thus likely unmasking a normally transient interaction of the POK1-TAN protein complex with MTs (Figure 3). This observation raises the exciting possibility that the CDZ resident POK1-TAN complex might indeed stabilize transient interactions with phragmoplast emanating MTs that approach the CDS to direct the phragmoplast/cell plate to its final destination.

Intriguingly, the localization pattern of POK1 is complementary to that of the cell cycle–regulated kinesin-14, KCA1 (Vanstraelen et al., 2006). KCA1 interacts with PPB-localized CDKA;1 (Vanstraelen et al., 2006), the MT severing protein katanin (Boutté et al., 2010) and the actin cytoskeleton (Suetsugu et al., 2010). *kca1 kca2* double mutants are primarily affected in chloroplast movement (Suetsugu et al., 2010). The predicted MT minus end directed motor activity of KCA1 seems well suited to accomplish a cortical pulling force to orient a mitotic MT array, similar to dynein, which is required for spindle/division plane orientation in animals (Kiyomitsu and Cheeseman, 2013). The complementary localization at the plasma membrane of two sets of kinesins leads to the intriguing hypothesis that the KCA and POK kinesin proteins might act antagonistically to position/guide mitotic MT arrays. However, the role of KCA1 in division plane orientation awaits further scrutiny.

The overall phenotype of *pok1-1 pok2-3* seedlings is strikingly similar to weak alleles of *ton2* (Kirik et al., 2012; Spinner and Gadeyne et al., 2013). Intriguingly, the POK-independent TAN and RanGAP1 recruitment to the CDZ correlates with the presence of TON2 at the CDZ, which disappears from the CDZ upon anaphase, as was shown for the TON2 homolog DCD1 in maize (Wright et al., 2009) and for *Arabidopsis* TON1 and FASS (Spinner et al., 2013). Interestingly, the MAPK cascade controlling MT turnover in the expanding phragmoplast is initiated by interaction of the HINKEL/At-NACK1 kinesin with the respective MAPKKK NPK1. Phosphorylation of both proteins by CDKs prevents their binding, while their dephosphorylation at the metaphase/anaphase transition is critically required for successful cytokinesis (Sasabe et al., 2011). Similarly, phosphoregulation might direct the anchoring of POK1 at the cell cortex upon PPB disassembly and/or control the binding of TAN and POK1 involving TON2-dependent dephosphorylation. Indeed, TAN is a potential target of phosphoregulation, as pharmacological inhibition of phosphatases as well as genetic interference with TON2 function prevented its cortical localization (Walker et al., 2007; Rasmussen et al., 2011).

In summary, we provide evidence for POK's critical function for the maintenance of CDZ/CDS identity. In a MT-dependent

manner, dynamic POK1 is continuously recruited to the CDZ during prophase, most likely from a cytoplasmic pool that is depleted prior to metaphase. Upon its arrival at the CDZ, POK1 becomes immobilized and subsequently its localization narrows by a yet unknown mechanism as mitosis progresses (Figure 7). Independent from POK function, TAN and RanGAP1 arrive at the CDZ, where they become tethered by a POK-dependent mechanism possibly involving TON2-mediated dephosphorylation of TAN (Figure 7).

Together, these proteins provide positional information of the division plane and might even actively participate in the phragmoplast guidance mechanism. However, at this point it still remains to be elucidated whether POKs are actively engaged in the phragmoplast guidance mechanism or whether their function is primarily a scaffolding activity to provide a spatial reference for CDZ components following PPB disassembly. Future studies are geared toward resolving these open questions.

METHODS

Plant Material

Arabidopsis thaliana plants, accession Columbia, were used throughout the study unless otherwise indicated. SALK T-DNA insertion lines for *pok1-1*, *pok1-2*, *pok2-1*, and *pok2-2*, as well as the double mutants *pok1-1 pok2-1* and *pok1-2 pok2-2*, have been described previously (Müller et al., 2006). *Agrobacterium tumefaciens*–mediated transformation to create diverse transgene lines was performed according to Clough and Bent (1998).

Growth Conditions

For examination of mutant phenotypes and localization studies at the seedling stage, seedlings were grown on plates containing Murashige and Skoog basal medium (Sigma-Aldrich) and 1% agarose or agar. For reproduction and crossing, plants were grown in soil. Plates and pots were incubated at 20 to 22°C on a 16-h-light/8-h-dark cycle.

Ethyl Methanesulfonate Mutagenesis and Identification of *pok2-3*

Plants homozygous for the *pok1-1* mutation where imbibed in deionized water, mutagenized with 0.3% ethyl methanesulfonate overnight, and thoroughly washed subsequently. Five-hundred M1 progeny were scored for short roots on standard Murashige and Skoog medium plates, and seeds were collected individually for each M1 plant. Among eight preselected M2 families, one segregated the *pok1-1 pok2-3* phenotype. We performed test crosses with *pok1-1 pok2-1* and since the progeny (n = 120) showed the *pok1 pok2* phenotype, we concluded that *POK2* was mutated. Sequencing of the *POK2* locus identified a C-to-T substitution in exon 16 leading to a premature stop codon.

Microtubule Marker Line

The MT binding domain MBD contained in a Gateway (Invitrogen) compatible destination vector pEG104-*Pro35S*:mCherry-MBD (Gutierrez et al., 2009) was recombined into pDONR207 (Invitrogen) by the BP clonase reaction. Subsequently, the LR reaction was performed with the destination vector *pUBN*:RFP containing the *Arabidopsis* Ubiquitin10 promoter (Grefen et al., 2010). Transgenic plant lines expressing XFP-MBD fusion protein have been used as a faithful MT marker (Marc et al., 1998; Gutierrez et al., 2009).

Generation of YFP-POK1 Fusion Protein

A recombineering-based approach was used to genetically insert the YFP tag at the 5′ of *POK1*. All recombineering steps were essentially performed as described (Tursun et al., 2009). In brief, recombineering primers (Supplemental Table 1) encoding 50 nucleotides of POK1 homology arms immediately upstream and downstream of the ATG and ~50 nucleotides of a plasmid pBALU6 (Tursun et al., 2009), containing a YFP and GalK cassette, were used to amplify the fluorophore and the GalK selection marker. The binary BAC 79I20 carrying the genomic region of *POK1* was transformed into *Escherichia coli* strain SW105, which allowed homologous recombination upon heat induction. Electro-competent SW105 containing BAC 79I20 were incubated at 42°C for 15 min to induce λ *red* recombinase and subsequently transformed with the PCR product amplified from the YFP-GalK cassette. Then cells were propagated for 3 h at 32°C and plated on galactose minimal medium. Colonies were streaked on McConkey indicator plates to screen for galactokinase activity, which lead to changes in pH of the medium turning colonies pink. Positive clones were further analyzed by PCR for the integration of the cassette into the BAC. Selected clones were cultured in liquid medium and split after propagation. One aliquot was supplied with 1/100 volume of 10% arabinose solution for induction of FLP recombinase to remove the GalK selection marker. Both aliquots were propagated for two additional hours before DNA was extracted. Induced and noninduced samples were analyzed by PCR with primers (Supplemental Table 1) flanking the recombination site. Clones where GalK was efficiently excised were sequence verified and used for transformation into *Agrobacterium* strain GV3101. After *Arabidopsis* transformation, five independent T1 lines were recovered on nutrient agar plates containing 0.05% phosphinotrycin, and T2 plants were inspected for YFP-POK1 localization. Two independent T2 lines showed YFP fluorescence and were selected for further analysis. Both lines rescued the *pok1 pok2* double mutant phenotype and showed an identical localization pattern of the YFP-POK1 fusion protein in Columbia and *pok1 pok2* rescue plants.

TAN with and without stop codon was amplified from full-length cDNA clones obtained from the RIKEN institute (pda14314) (primers are listed in Supplemental Table 2). Because these primers were flanked with the minimal attB sites, all PCR products were amplified with the full-length attB1F and attB2R primers (Supplemental Table 2) and cloned into pDONR221 via a Gateway BP reaction (Invitrogen). $POK1_{1213\text{-}2066}$ coding sequences with and without stop codon were amplified from entry clone pENTR-POK1 described by Xu et al. (2008).

The dTom-$POK1_{1265\text{-}2066}$ fusion construct was created in the pK7m34GW vector (Karimi et al., 2007) using the dTomato coding sequence and the POK cDNA fragment corresponding to amino acids 1265 to 2066 (Supplemental Table 3) under control of the constitutive promoter from the At3g16640 gene (Berkowitz et al., 2008).

The short-terminal fragment $POK1_{1683\text{-}2066}$ was cloned into pENTR3C via *Eco*RI/*Xho*I from pAD-POK1C (Müller et al., 2006) and recombined with pEG104 (Earley et al., 2006) to create *Pro35S:YFP-POK1*$_{1683\text{-}2066}$.

Pro35S:RFP-MBD expressed in BY-2 cells was described elsewhere (Marc et al., 1998; Van Damme et al., 2004). Entry clones of $POK1C_{1213\text{-}2066}$ and TAN with stop codon (Supplemental Table 2) were used in a single Gateway LR reaction with pK7WGF2 to generate N-terminal GFP fusion proteins. Entry clones of POK1C without stop codon were combined with pK7FWG2 to create C-terminal GFP fusion proteins.

Subcellular distribution of YFP-POK1 signal (Supplemental Figure 5) was analyzed in indirect immunolocalization experiments using anti-GFP (Invitrogen) and antitubulin (YL1/2; Abcam) and secondary antibodies anti-rabbit-Alexa488 (Invitrogen) and anti-rat-Cy3 (Jackson Immuno Research).

Confocal Imaging and Image Processing

Imaging was performed on a Leica SP2 equipped with a point scanner and a Leica SP8 confocal microscope equipped with a resonant scanner.

A 63×, numerical aperture (NA) = 1.20, water immersion objective lens was used for image acquisition. YFP fluorescence was excited by the 514-nm laser line from an argon/krypton laser and detected with a standard PMT on the SP2 or a HyD detector on the SP8 set to a detection window between 520 and 550 nm. RFP was excited with a 561-nm He/Ne laser, and fluorescence was detected with a standard PMT or a HyD detector set at 570 to 650 nm. GFP was excited with a 488-nm laser line from an argon/krypton laser and detected with a PMT or a HyD detector at 500 to 550 nm.

BY-2 cells were imaged on an Olympus FV1000 inverted confocal microscope equipped with a water-corrected 60× objective (NA = 1.2) using a 488-nm laser excitation and a spectral detection bandwidth of 500 to 530 nm for enhanced GFP and a 559-nm laser excitation together with a spectral detection bandwidth of 570 to 670 nm for RFP detection and with a Zeiss 710 inverted confocal microscope with the ZEN 2009 software package and equipped with a 63× water-corrected objective (NA = 1.2). GFP was visualized using 488-nm laser excitation and 500- to 530-nm spectral detection; RFP was visualized using 458-nm laser excitation and 592- to 754-nm spectral detection.

Two-dimensional projections and three-dimensional reconstructions of Z stacks were generated with either ImageJ v.1.48a (http://rsb.info.nih.gov/ij/) or Leica LF Image processing. Color merges were performed with NIH ImageJ v.1.48s or Adobe Photoshop CS5 v12.0.4 (Adobe Systems). Only linear adjustments to pixel values were applied.

To determine the duration of cytokinesis and the orientation of phragmoplasts (transverse versus torus view), a *pok1-1 pok2-3* segregating population derived from a cross with the GFP-MBD marker line described by Marc et al. (1998) was used. Time-lapse imaging of cells displaying spindle stages was performed and continued throughout mitosis at 3- to 5- min intervals. Time intervals were shorter at the beginning of the time lapse to determine the transition from spindle to phragmoplast and at the end of cytokinesis, while longer interval times were chosen during phragmoplast expansion. The duration was timed from the spindle/phragmoplast transition until phragmoplast disassembly.

The rate of phragmoplast expansion was determined using kymograph analysis (Buschmann et al., 2010). We recorded time-lapse images of cells displaying spindles or earlier cell cycle stages at 2.5-min intervals until the phragmoplast made contact with the cell wall. In ImageJ, the segmented line tool was used to select the distance for the measurement, spanning the diameter of the phragmoplast. To determine relative velocities and to visualize the narrowing of the POK1C or TAN localization at the CDZ, the ImageJ kymograph plug-in (http://www.embl.de/eamnet/html/body_kymograph.html) was used. Based on these measurements, the velocities of phragmoplast expansion were calculating in Excel.

Ratiometric BiFC

The ratiometric BiFC Gateway-compatible 2in1 system (Grefen and Blatt, 2012) was used to examine interaction between $POK1_{1683\text{-}2066}$ and TAN. ROP2 was used as a negative control since, like POK1, it localized to the plasma membrane. The potential binding partners were expressed under the control of the Pro35S promoter on the same plasmid, which also carries RFP as an internal expression control. The ratio between YFP and RFP is used to estimate interaction strength. The primers used to amplify the cDNA of binding partners are listed in Supplemental Table 2. Amplicons were cloned via the BP reaction into pDONR221-P1P4 or pDONr221-P2P3. The resulting entry clones were used in subsequent LR reactions with destination vector pBiFCt-2in1-NN. All steps were performed according to Grefen and Blatt (2012). Protoplasts from *Arabidopsis* suspension culture were transformed with the pBiFCt-2in1-NN plasmids according to Schütze et al. (2009). YFP and RFP fluorescence were excited with 514- and 561-nm excitation wavelength by sequential scan using the Leica TCS SP8 resonant scanner and hybrid detector HyD2 set to 518 to 552 nm for YFP fluorescence and PMT4 set to 645 to 731 nm for RFP fluorescence. All images were taken at identical settings. Quantification of fluorescence intensity was performed in ImageJ. The segmented line tool, set to a 7.5-pixel width, was used to trace the protoplasts and mean fluorescence intensity was measured along this line. Calculation of mean YFP/RFP ratio and the graph were performed in Excel. The mCherry-ROP2 control was generated using CreLox according to Geldner et al. (2009) via recombination of *pUNI-ROP2* with pNIGL17. As localization control for TAN, the plasmid *pEZRK:TAN-YFP* described by Walker et al. (2007) was used.

BY-2 Transformation

Stable BY-2 transformation was performed as described before (Geelen and Inzé, 2001). BY-2 cell lines expressing two fluorescent constructs were created by consecutive supertransformation of single transformed lines. Stably transformed calli were screened for fluorescence and localization patterns of tagged proteins were confirmed by analyzing several independent transformants.

FRAP Analysis

FRAP experiments for the POK1 C-terminal fragment $GFP\text{-}POK1_{1213\text{-}2066}$ were conducted on an Olympus FluoView1000 inverted confocal microscope. One prebleach images was taken. A certain region of interest (ROI) was bleached for 10 s with 100% laser power. Subsequent images were taken every 60 s. BY-2 cells were mounted in a chambered cover glass system (Lab-Tek) in 1% low melting point agarose containing BY-2 medium.

The average fluorescence intensity of the bleached region (ROI1) was measured using ImageJ [I(t)]. The position of ROI1 was adjusted manually during the time lapse to correct for cell drifting. The average intensity of a second ROI (ROI2) outside the cell was measured to compensate for background fluorescent signal (Ibase). Because Ibase approaches a constant value, we subtracted the average Ibase from I(t) to obtain the actual fluorescence intensity Ifrap(t) (I(t)-average(Ibase) = Ifrap(t)). To estimate the amount of photobleaching due to image acquisition, we measured the average intensity of the whole cell (ROI3). From these values we also subtracted the background signal (average Ibase). These values were set out in a scatterplot and fitted to a linear trendline, which allowed us to determine the theoretical reduction in fluorescence intensity due to image acquisition for each time point (Ibleach(t)).

To obtain a normalized value for fluorescence recovery (Inorm(t)), we first determined the ratio of fluorescence loss due to image acquisition:

$$\mathrm{Ibleach}(t=0)/\mathrm{Ibleach}(t) \quad (1)$$

Next, the remaining fluorescence intensity after photobleaching (Ifrap(post)) was set to zero and all intensity values were adjusted accordingly:

$$\mathrm{Ifrap}(t) - \mathrm{Ifrap}(\mathrm{post}) \quad (2)$$

$$\mathrm{Ifrap}(t=0) - \mathrm{Ifrap}(\mathrm{post}) \quad (3)$$

Finally, to obtain the normalized values for fluorescence recovery after photobleaching (Inorm(t)), the previous equations were combined as follows:

$$\mathrm{Inorm}(t) = (1)^{*}((2)/(3))$$

The average Inorm(t) (FRAP, Figure 6D, prophase cells, $n = 4$; metaphase cells, $n = 7$; FRAP, Figure 6L, $n = 6$) was set out in a scatterplot using Sigmaplot 12. A single exponential regression with rise to a maximum (y = a*(1-exp(-b*t))) was fitted to the data points. The half-time ($t_{1/2}$) for fluorescence recovery was calculated using the above formula with the fluorescence intensity value corresponding to half of the fitted maximum recovery at the latest time point as y.

FRAP experiments of full-length YFP-POK1 were performed using 4- to 7-d-old seedlings expressing *ProPOK1*:YFPgPOK1 in the *pok1-1 pok2-3* background. Seedlings were mounted in water on solid half-strength nutrient (0.5× Murashige and Skoog salt, 1.5% agar). Using the

Leica SP8, four prebleach images were taken, and then the selected ROI (ROI1) was bleached with identical laser settings for each experiment. Fluorescent signal recovery was imaged at 60-s time intervals for 30 min. FRAP data analysis was performed as described for GFP-POK1C. The background was determined outside of the root (ROI2), and the average intensity of the whole cell (ROI3) was used to correct for photobleaching during image acquisition without trendline fitting.

Oryzalin Treatment

Four- to five-day-old seedlings coexpressing YFP-POK1 and RFP-MBD were imaged and subsequently treated by exchanging mounting medium with 10 μM oryzalin solution. Fluorescence of cells that had PPBs, spindles, or phragmoplasts and YFP-POK1 prior to oryzalin treatment were reanalyzed at 5-min intervals for 10 to 30 min. BY-2 cells were mounted in a chambered cover glass system (Lab-Tek). Cells were immobilized in a thin layer (1 mL) of BY-2 medium containing vitamins (Geelen and Inzé 2001), 0.8 to 1% low melting point agarose (Invitrogen) and 10 μM oryzalin. BY-2 cells were imaged to the point where MT depolymerization was evident followed by FRAP analysis.

Accession Numbers

Sequence data from this article can be found in the Arabidopsis Genome Initiative or GenBank/EMBL databases under the following accession numbers: At3g17360, POK1; At3g19050, POK2; and At3g05330, TAN1.

Supplemental Data

The following materials are available in the online version of this article.

Supplemental Figure 1. Adult Phenotype of *pok1 pok2* and Rescue with YFP-POK1.

Supplemental Figure 2. Mitotic Microtubule Arrays in *pok1-1 pok2-3* Mutants.

Supplemental Figure 3. Cell Cycle Progression.

Supplemental Figure 4. Subcellular Localization of Different Fluorescent POK1 Fusions.

Supplemental Figure 5. Subcellular Distribution of YFP-POK1 Signal in *Arabidopsis* Mitotic Cells.

Supplemental Figure 6. Examples of Transient Microtubules Reaching from the Phragmoplast toward the Putative Cortical Division Site.

Supplemental Table 1. Primers Used for Cloning Full-Length YFP-POK1 and Genotyping of *pok1-1*.

Supplemental Table 2. List of Primers Used for Cloning 2in1 Plasmids.

Supplemental Table 3. List of Primers Used for Cloning.

Supplemental Movie 1. Time Lapse of Wild-Type Cell Division.

Supplemental Movie 2. Time Lapse of *pok1-1 pok2-3* Cell Division.

Supplemental Movie Legends.

Supplemental Movie 1. Time Lapse of Wild-Type Cell Division at 1.5 fps.

Supplemental Movie 2. Time Lapse of *pok1-1 pok2-3* Cell Division at 1.5 fps.

ACKNOWLEDGMENTS

We acknowledge the ABRC and NASC for distribution of seed used in this study. The instructive advice and provision of *E. coli* SW105 and the recombineering plasmid collection by Baris Tursun is gratefully acknowledged. We thank Christopher Grefen for advice and the ratiometric BiFC plasmids. We thank Daniela Daumüller, Phillip Reichert, Hs Lee, Richard Gavidia, Angela Kirik, and Samantha Atkinson for help with data collection. We thank Katharina Brancato from the ZMBP Transformation service. We appreciate the support from the Department of Developmental Genetics lead by Gerd Jürgens. Funding for this work was provided by Deutsche Forschungsgemeinschaft grants to S.M. (DFG MU 3133/1-1 and SFB1101) and by a National Institutes of Health grant (1R15GM102839)-01A1 (V.K.). A.G. was indebted to the Agency for Innovation by Science and Technology for a predoctoral fellowship.

AUTHOR CONTRIBUTIONS

E.L., A.G., D.V.D., G.D.J., D.E., V.K., and S.M. designed the research. E.L., A.G., D.S., S.Z., D.V.D., V.K., and S.M. performed research. E.L., A.G., D.S., D.V.D., V.K., and S.M. analyzed data. D.V.D. and S.M. wrote the article.

Received March 3, 2014; revised May 14, 2014; accepted June 6, 2014; published June 27, 2014.

REFERENCES

Ambrose, J.C., Shoji, T., Kotzer, A.M., Pighin, J.A., and Wasteneys, G.O. (2007). The *Arabidopsis* CLASP gene encodes a microtubule-associated protein involved in cell expansion and division. Plant Cell **19:** 2763–2775.

Berkowitz, O., Jost, R., Pollmann, S., and Masle, J. (2008). Characterization of TCTP, the translationally controlled tumor protein, from *Arabidopsis thaliana*. Plant Cell **20:** 3430–3447.

Boutté, Y., Frescatada-Rosa, M., Men, S., Chow, C.M., Ebine, K., Gustavsson, A., Johansson, L., Ueda, T., Moore, I., Jürgens, G., and Grebe, M. (2010). Endocytosis restricts Arabidopsis KNOLLE syntaxin to the cell division plane during late cytokinesis. EMBO J. **29:** 546–558.

Buschmann, H., Sambade, A., Pesquet, E., Calder, G., and Lloyd, C.W. (2010). Microtubule dynamics in plant cells. Methods Cell Biol. **97:** 373–400.

Camilleri, C., Azimzadeh, J., Pastuglia, M., Bellini, C., Grandjean, O., and Bouchez, D. (2002). The *Arabidopsis TONNEAU2* gene encodes a putative novel protein phosphatase 2A regulatory subunit essential for the control of the cortical cytoskeleton. Plant Cell **14:** 833–845.

Cleary, A.L., and Smith, L.G. (1998). The *Tangled1* gene is required for spatial control of cytoskeletal arrays associated with cell division during maize leaf development. Plant Cell **10:** 1875–1888.

Cleary, A.L., Gunning, B.E.S., Wasteneys, G.O., and Hepler, P.K. (1992). Microtubule and F-actin dynamics at the division site in living tradescantia stamen hair cells. J. Cell Sci. **103:** 977–988.

Clough, S.J., and Bent, A.F. (1998). Floral dip: a simplified method for Agrobacterium-mediated transformation of *Arabidopsis thaliana*. Plant J. **16:** 735–743.

De Rybel, B., Möller, B., Yoshida, S., Grabowicz, I., Barbier de Reuille, P., Boeren, S., Smith, R.S., Borst, J.W., and Weijers, D. (2013). A bHLH complex controls embryonic vascular tissue establishment and indeterminate growth in Arabidopsis. Dev. Cell **24:** 426–437.

Dhonukshe, P., and Gadella, T.W., Jr., (2003). Alteration of microtubule dynamic instability during preprophase band formation

revealed by yellow fluorescent protein-CLIP170 microtubule plus-end labeling. Plant Cell **15:** 597–611.

Earley, K.W., Haag, J.R., Pontes, O., Opper, K., Juehne, T., Song, K., and Pikaard, C.S. (2006). Gateway-compatible vectors for plant functional genomics and proteomics. Plant J. **45:** 616–629.

Endow, S.A., Kull, F.J., and Liu, H. (2010). Kinesins at a glance. J. Cell Sci. **123:** 3420–3424.

Geelen, D.N.V., and Inzé, D.G. (2001). A bright future for the bright yellow-2 cell culture. Plant Physiol. **127:** 1375–1379.

Geldner, N., Dénervaud-Tendon, V., Hyman, D.L., Mayer, U., Stierhof, Y.-D., and Chory, J. (2009). Rapid, combinatorial analysis of membrane compartments in intact plants with a multicolor marker set. Plant J. **59:** 169–178.

Gorst, J., Wernicke, W., and Gunning, B.E.S. (1986). Is the preprophase band of microtubules a marker of organization in suspension-cultures. Protoplasma **134:** 130–140.

Grefen, C., and Blatt, M.R. (2012). A 2in1 cloning system enables ratiometric bimolecular fluorescence complementation (rBiFC). Biotechniques **53:** 311–314.

Grefen, C., Donald, N., Hashimoto, K., Kudla, J., Schumacher, K., and Blatt, M.R. (2010). A ubiquitin-10 promoter-based vector set for fluorescent protein tagging facilitates temporal stability and native protein distribution in transient and stable expression studies. Plant J. **64:** 355–365.

Gunning, B.E.S., and Wick, S.M. (1985). Preprophase bands, phragmoplasts, and spatial control of cytokinesis. J. Cell Sci. Suppl. **2:** 157–179.

Gutierrez, R., Lindeboom, J.J., Paredez, A.R., Emons, A.M., and Ehrhardt, D.W. (2009). Arabidopsis cortical microtubules position cellulose synthase delivery to the plasma membrane and interact with cellulose synthase trafficking compartments. Nat. Cell Biol. **11:** 797–806.

Karimi, M., Depicker, A., and Hilson, P. (2007). Recombinational cloning with plant gateway vectors. Plant Physiol. **145:** 1144–1154.

Kirik, A., Ehrhardt, D.W., and Kirik, V. (2012). TONNEAU2/FASS regulates the geometry of microtubule nucleation and cortical array organization in interphase Arabidopsis cells. Plant Cell **24:** 1158–1170.

Kirik, V., Herrmann, U., Parupalli, C., Sedbrook, J.C., Ehrhardt, D.W., and Hülskamp, M. (2007). CLASP localizes in two discrete patterns on cortical microtubules and is required for cell morphogenesis and cell division in Arabidopsis. J. Cell Sci. **120:** 4416–4425.

Kiyomitsu, T., and Cheeseman, I.M. (2013). Cortical dynein and asymmetric membrane elongation coordinately position the spindle in anaphase. Cell **154:** 391–402.

Lau, S., Slane, D., Herud, O., Kong, J., and Jürgens, G. (2012). Early embryogenesis in flowering plants: setting up the basic body pattern. Annu. Rev. Plant Biol. **63:** 483–506.

Lee, Y.R., and Liu, B. (2004). Cytoskeletal motors in Arabidopsis. Sixty-one kinesins and seventeen myosins. Plant Physiol. **136:** 3877–3883.

Lipka, E., and Müller, S. (2012). Potential roles for kinesins at the cortical division site. Front. Plant Sci. **3:** 158.

Marc, J., Granger, C.L., Brincat, J., Fisher, D.D., Kao, Th., McCubbin, A.G., and Cyr, R.J. (1998). A GFP-MAP4 reporter gene for visualizing cortical microtubule rearrangements in living epidermal cells. Plant Cell **10:** 1927–1940.

Mineyuki, Y., and Palevitz, B.A. (1990). Relationship between preprophase band organization, F-actin and the division site in Allium: fluorescence and morphometric studies on cytochalasin-treated cells. J. Cell Sci. **97:** 283–295.

Müller, S., Han, S., and Smith, L.G. (2006). Two kinesins are involved in the spatial control of cytokinesis in *Arabidopsis thaliana*. Curr. Biol. **16:** 888–894.

Paredez, A.R., Somerville, C.R., and Ehrhardt, D.W. (2006). Visualization of cellulose synthase demonstrates functional association with microtubules. Science **312:** 1491–1495.

Pickett-Heaps, J.D., and Northcote, D.H. (1966). Organization of microtubules and endoplasmic reticulum during mitosis and cytokinesis in wheat meristems. J. Cell Sci. **1:** 109–120.

Pietra, S., Gustavsson, A., Kiefer, C., Kalmbach, L., Hörstedt, P., Ikeda, Y., Stepanova, A.N., Alonso, J.M., and Grebe, M. (2013). Arabidopsis SABRE and CLASP interact to stabilize cell division plane orientation and planar polarity. Nat. Commun. **4:** 2779.

Rasmussen, C.G., Sun, B., and Smith, L.G. (2011). Tangled localization at the cortical division site of plant cells occurs by several mechanisms. J. Cell Sci. **124:** 270–279.

Rasmussen, C.G., Wright, A.J., and Müller, S. (2013). The role of the cytoskeleton and associated proteins in determination of the plant cell division plane. Plant J. **75:** 258–269.

Rodrigo-Peiris, T., Xu, X.M., Zhao, Q., Wang, H.-J., and Meier, I. (2011). RanGAP is required for post-meiotic mitosis in female gametophyte development in *Arabidopsis thaliana*. J. Exp. Bot. **62:** 2705–2714.

Sano, T., Higaki, T., Oda, Y., Hayashi, T., and Hasezawa, S. (2005). Appearance of actin microfilament 'twin peaks' in mitosis and their function in cell plate formation, as visualized in tobacco BY-2 cells expressing GFP-fimbrin. Plant J. **44:** 595–605.

Sasabe, M., Boudolf, V., De Veylder, L., Inzé, D., Genschik, P., and Machida, Y. (2011). Phosphorylation of a mitotic kinesin-like protein and a MAPKKK by cyclin-dependent kinases (CDKs) is involved in the transition to cytokinesis in plants. Proc. Natl. Acad. Sci. USA **108:** 17844–17849.

Schütze, K., Harter, K., and Chaban, C. (2009). Bimolecular fluorescence complementation (BiFC) to study protein-protein interactions in living plant cells. In Plant Signal Transduction, T. Pfannschmidt, ed (Totowa, NJ: Humana Press), pp. 189–202.

Smith, L.G., Gerttula, S.M., Han, S., and Levy, J. (2001). Tangled1: a microtubule binding protein required for the spatial control of cytokinesis in maize. J. Cell Biol. **152:** 231–236.

Smith, L.G., Hake, S., and Sylvester, A.W. (1996). The tangled-1 mutation alters cell division orientations throughout maize leaf development without altering leaf shape. Development **122:** 481–489.

Spinner, L., et al. (2013). A protein phosphatase 2A complex spatially controls plant cell division. Nat. Commun. **4:** 1863.

Suetsugu, N., Yamada, N., Kagawa, T., Yonekura, H., Uyeda, T.Q.P., Kadota, A., and Wada, M. (2010). Two kinesin-like proteins mediate actin-based chloroplast movement in *Arabidopsis thaliana*. Proc. Natl. Acad. Sci. USA **107:** 8860–8865.

Torres-Ruiz, R.A., and Jürgens, G. (1994). Mutations in the FASS gene uncouple pattern formation and morphogenesis in Arabidopsis development. Development **120:** 2967–2978.

Traas, J., Bellini, C., Nacry, P., Kronenberger, J., Bouchez, D., and Caboche, M. (1995). Normal differentiation patterns in plants lacking microtubular preprophase bands. Nature **375:** 676–677.

Tursun, B., Cochella, L., Carrera, I., and Hobert, O. (2009). A toolkit and robust pipeline for the generation of fosmid-based reporter genes in C. elegans. PLoS ONE **4:** e4625.

Van Damme, D. (2009). Division plane determination during plant somatic cytokinesis. Curr. Opin. Plant Biol. **12:** 745–751.

Van Damme, D., Van Poucke, K., Boutant, E., Ritzenthaler, C., Inzé, D., and Geelen, D. (2004). In vivo dynamics and differential microtubule-binding activities of MAP65 proteins. Plant Physiol. **136:** 3956–3967.

Vanstraelen, M., Van Damme, D., De Rycke, R., Mylle, E., Inzé, D., and Geelen, D. (2006). Cell cycle-dependent targeting of a kinesin at the plasma membrane demarcates the division site in plant cells. Curr. Biol. **16:** 308–314.

Vos, J.W., Dogterom, M., and Emons, A.M. (2004). Microtubules become more dynamic but not shorter during preprophase band formation: a possible "search-and-capture" mechanism for microtubule translocation. Cell Motil. Cytoskeleton **57:** 246–258.

Walker, K.L., Müller, S., Moss, D., Ehrhardt, D.W., and Smith, L.G. (2007). Arabidopsis TANGLED identifies the division plane throughout mitosis and cytokinesis. Curr. Biol. **17:** 1827–1836.

Wright, A.J., Gallagher, K., and Smith, L.G. (2009). discordia1 and alternative discordia1 function redundantly at the cortical division site to promote preprophase band formation and orient division planes in maize. Plant Cell **21:** 234–247.

Xu, X.M., Zhao, Q., Rodrigo-Peiris, T., Brkljacic, J., He, C.S., Müller, S., and Meier, I. (2008). RanGAP1 is a continuous marker of the Arabidopsis cell division plane. Proc. Natl. Acad. Sci. USA **105:** 18637–18642.